Journal of Manufacturing Processes 107 (2023) 166–178

Contents lists available at ScienceDirect

Journal of Manufacturing Processes

journal homepage: www.elsevier.com/locate/manpro

Tuning of SiO_2/Si interface by a hybrid plasma process combining oxidation and atom-migration

Shaoxiang Liang [a], Bing Wu [a], Yinhui Wang [a,*], Hui Deng [a,b,**]

[a] Department of Mechanical and Energy Engineering, Southern University of Science and Technology, Shenzhen, Guangdong 518055, PR China
[b] Institute for Applied Optics and Precision Engineering, Southern University of Science and Technology, Shenzhen, Guangdong 518055, PR China

ARTICLE INFO

Keywords:
SiO_2/Si interface
Plasma
Atomic level
Oxidation
Atom migration
Roughness

ABSTRACT

As a common oxide-semiconductor interface, SiO_2/Si plays an important role in silicon-based electronics and optoelectronics. In order to effectively obtain an ultra-smooth and thin SiO_2/Si interface, a hybrid tuning process based on inductively coupled plasma (ICP) was proposed, which combined oxidation (plasma-OX) and atom-migration manufacturing (plasma-AMM). In plasma-OX process, a thick oxide film was rapidly prepared on Si wafer surface in 2 min, which included a SiO_2 layer on the top and a SiO_x ($x < 2$) layer between the top layer and the bulk crystalline silicon (*c*-Si). In subsequent plasma-AMM process, ICP steadily delivered energy to the Si wafer surface and induced the migration of unsaturated Si from SiO_x layer to *c*-Si, which enhanced the crystallization of silicon wafer. The roughness of SiO_2/Si interface was reduced to *Sa* 0.171 nm at 620 W in 5 min. However, a 2–3 nm thickness SiO_x layer still existed, and several defects causing by residual thermal stress can be observed. Further optimizing plasma-AMM process by setting multi-step slow cooling, the SiO_x layer can be almost completely decomposed. The interface roughness *Sa* was reduced to <0.1 nm and the interface thickness was reduced to 1–2 atom layer. Both OX and AMM process were conducted in the same setup, which is convenient for switching. This study proposed and demonstrated the feasibility of a hybrid plasma tuning process, which provided an efficient tuning technology at atomic level for semiconductor interface.

1. Introduction

Interface is a key component of Metal-Oxide-Semiconductor Field-Effect Transistor (MOSFET), which has a wide range of applications in modern electronics and optoelectronics. The fabrication and the performance analysis of these interfaces, such as Nb/Hf/Ti/Oxide [1], Al/Al_2O_3 [2,3], HfO_x/Hf [4], SiO_2/Si [5,6], and GeO_2/Ge [7,8], are particularly important in the technology and application of advanced material, including functional ceramics material, metal coatings, catalysts and others [9].

As the most typical oxide-semiconductor interface, SiO_2/Si is closely related to the generation of oxide charges and states on the device surface [10,11]. The requirement for miniaturization of components has placed more stringent demands on ultra-thin oxide technology, which means that it is necessary to understand and control the laws of SiO_2/Si interface formation at the atomic level and a smooth and thin SiO_2/Si interface at atomic level with low-defect was needed [12,13]. Also, the rapid developments of lithography technology [14] and Si quantum computing [15,16] put forward more strict demands on the surface of Si semiconductor [17,18]. Along with the increasing requirement on manufacturing accuracy, the atomic and close-to-atomic scale manufacturing (ACSM) [19–21] was proposed, in which the materials are removed, transferred or added at the atomic level. Thus, ACSM will be the research focus in advanced surface/interface manufacturing of semiconductor.

As early as 1978, Krivanek [22] proposed a smooth SiO_2/Si interface (0.4 nm) containing possible non-stoichiometric oxides as a transition layer. In the decades that followed, the SiO_2/Si interface was observed at micro/nanoscale [23,24]. Bongiorno [25] and Tu [26] proposed a method for the orderliness of the SiO_2/Si interface through quantitative and simulation calculations. The SiO_2/Si interface is not a simple contour morphology but a mixed SiO_x ($x < 2$) layer with a certain thickness.

Deal [27] discussed the relationship between SiO_2/Si interface structure and device characteristics in detail. They found that there was

* Corresponding author.
** Correspondence to: H. Deng, Institute for Applied Optics and Precision Engineering, Southern University of Science and Technology, Shenzhen, Guangdong 518055, PR China.
E-mail addresses: wangyh3@sustech.edu.cn (Y. Wang), dengh@sustech.edu.cn (H. Deng).

https://doi.org/10.1016/j.jmapro.2023.10.045
Received 3 August 2023; Received in revised form 12 October 2023; Accepted 13 October 2023
Available online 20 October 2023

a SiO_x ($x < 2$) oxide layer in the SiO_2/Si interface. The SiO_x layer contained partially ionized or excess Si, which could form new SiO_2 through diffusion reaction. Based on the reaction energies of different locations by first-principles calculation, Hiroyuki [28–30] investigated the behavior of the Si atoms migration and the reconstruction of SiO_2 layer. Bottomley reported that the atomic height steps at the SiO_2/Si (100) interface (~ 0.14 nm) were formed by annealing at ≥1325 °C [31]. In this process, the Si atoms in the SiO_x layer migrated and bonded to the *c*-Si during steady-state annealing. The evolution of interface morphology by mass transport can be quantitatively described by a surface self-diffusion mechanism [32]. A large number of investigations have confirmed that the flattened morphology [33,34], steps morphology [35,36] and spherical/columnar structures [37–40] were achieved by high temperature and annealing processes on the SiO_2/Si interface.

In our pervious works, a plasma-induced atomic migration manufacturing (plasma-AMM) process was proposed, which efficiently achieved ultra-smooth surface of fused silica based on inductively coupled plasma (ICP) [41,42]. The critical process of plasma-AMM is the instantaneous energy transfer to the wafer by ICP through three modes: thermal convection, heat conduction and thermal radiation. As the energy transferred continuously, the surface atoms received sufficient energy, broke bond and migrated in the surface. Until the migrated atoms reached to the low energy sites and the surface structure tended to be a balance state, an ultra-smoothing of surface was formed. Moreover, ICP is a typical strong ionized and equilibrium plasma, which exhibits the characteristics of high temperature and high particle concentration. The temperature of ICP can be adjusted within the range of hundreds to thousands of degrees, which could accurately control the processing temperature for the wafer. Therefore, ICP is an effective medium for inducing atomic migration, and plasma-AMM could be considered as a potential efficient process to control the reconstruction of SiO_2/Si interface.

In order to achieve an ultra-smooth and thin SiO_2/Si interface, an oxide film containing SiO_x was required on the Si wafer surface firstly before plasma-AMM process. By injecting oxygen into the ICP gas, the plasma oxidation (plasma-OX) reaction is expected to prepare a SiO_x layer rapidly under the high temperature, and it can be accomplished in the same setup of plasma-AMM. Considering the advantage and convenience of plasma-OX and plasma-AMM processes, an ultra-smooth and ultra-thin SiO_2/Si interface at atomic level may be processed by combining these two procedures. This study explored the plasma-OX manufacturing process and subsequent OX-AMM hybrid manufacturing process, respectively. Both of plasma-OX and plasma-AMM are based on atmosphere ICP setup, allowing flexible process switching. Then, an optimized plasma-AMM process by multi-step slow cooling was proposed to accomplish a SiO_2/Si interface of atomic thickness without defect, which is similar to laser annealing technology [43]. The core factors controlling the atomic migration in plasma-AMM process were investigated. The roughness evolution and morphology characteristics of SiO_2/Si interfaces were studied. An ultra-smooth and ultra-thin SiO_2/Si interface with ultimate precision was manufactured by the optimized OX-AMM hybrid process.

2. Mechanism and experimental procedures

Fig. 1 shows the schematic diagrams of plasma-OX and subsequent plasma-AMM process. As shown in Fig. 1(a), the original oxide film is derived from the natural oxidation in the atmospheric environment. In the normal temperature and pressure environment, the thickness of the natural oxide film is in low degree. When ICP containing abundant oxygen atoms irradiated on the Si surface, oxygen quickly permeated and diffused in the surface, which results in thickening the oxide layer in the plasma-OX process, as shown in Fig. 1(b). However, oxygen atoms cannot be completely matched up with Si atoms due to excessive oxygen permeation and short-term rapid oxidation. Thus, the plasma-OX processed oxide film consists of an oxygen-saturated layer (SiO_2) on the top

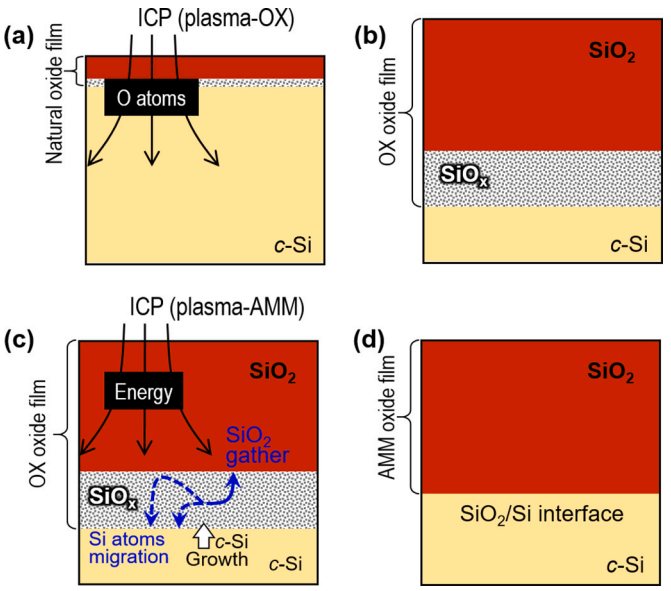

Fig. 1. The schematic diagrams of SiO_2/Si Interface during tuning plasma processing, (a) plasma-OX process, and (b) its surface layer structure after OX processing. (c) The subsequent plasma-AMM process, and (d) the interface after plasma-AMM process for Si wafer.

and an oxygen-unsaturated layer (SiO_x, $x < 2$) neighboring crystal silica (*c*-Si).

According to the results of high-temperature annealing for Si wafer, the roughness of the silicon surface decreased from 5.5 nm to 0.13 nm, and the surface lost the anisotropic nature during self-diffusion [32]. In this work, the plasma-AMM process may can achieve a similar function of high-temperature annealing because the plasma carries abundant thermal energy. As only argon is the reaction gas source, the physical influence mode for ICP was dominant in the plasma-AMM process [42], which was predicted to conduct the thermal repair of the SiO_2/Si interface.

Fig. 1(c) shows the atoms migration schematic diagram in the plasma-AMM process. Due to the continuous energy input from plasma, atoms in the SiO_x layer began to migrate. There likely are two paths for the atoms to migrate in the interfaces when the energy continuously input from plasma. One is that the unsaturated Si atoms in the SiO_x layer diffuse toward the SiO_2 layer with massive oxygen atoms, and the excessive O atoms in the top layer move downward to bond with Si atoms. The second is that the Si atoms migrate toward *c*-Si to extend the crystalline structure accompanying with some defects removing in crystalline silicon. During plasma-AMM processing, the burry interface for SiO_x gradually evolve to a distinguishable interface between SiOx and crystalline silicon structure because of the reconstruction of the bonding modes of Si atoms and O atoms, as shown in Fig. 1(d).

In this study, the plasma-OX process and subsequent plasma-AMM process on the Si surface were conducted on the same constructed equipment. Fig. 2(a) shows the ICP setup, which is mainly composed of RF (radio frequency) power supply, matcher, copper inductor coil, quartz torch tube, alumina sample table and three-axis computer numerical control (CNC) motion system. The torch tube is fixed at the center of the induction coil and consists of two coaxial quartz tubes (outer diameter 20 mm, inner diameter 16 mm). In OX process, the inner tube supplied a small flow of ignition gas (Ar) and reaction gas (O_2) and the outer tube supplied a large flow of cooling gas (Ar), which prevented quartz torches from melting at high temperatures and stabilized the plasma beam. With regards to the AMM mode, the supply of oxygen was stopped in the inner tube and others was same to plasma-OX process.

The surface temperature of Si wafer during the whole OX-AMM process was shown in Fig. 2(e). The material of the wafer samples in

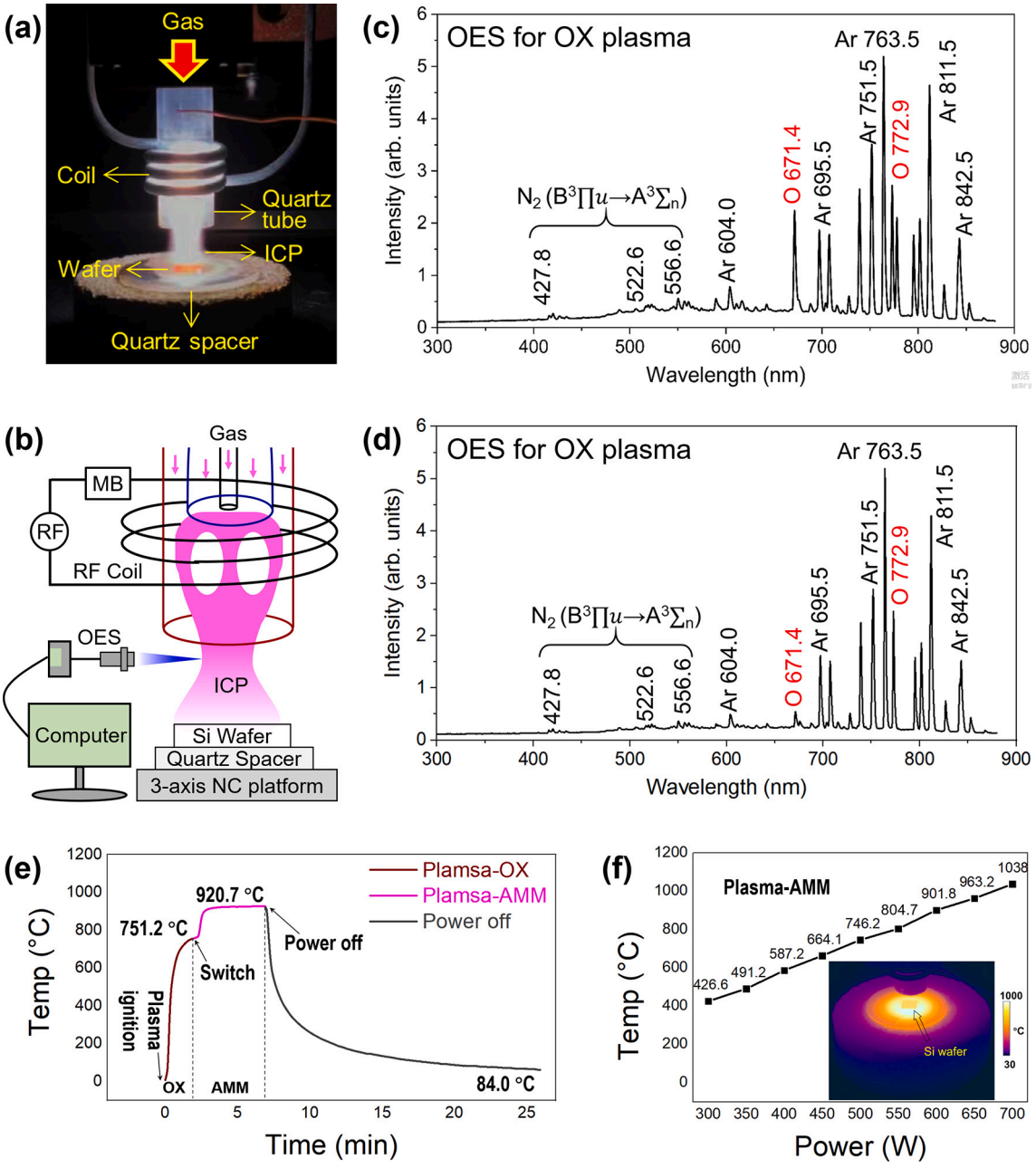

Fig. 2. (a) The photograph of ICP setup; (b) the schematic diagram of OES measurement for ICP diagnostic, the OES spectra obtained from plasma in (c) OX process and (d) AMM process; (e) the detected temperature of Si wafer surface during the whole OX-AMM process (RF power was 620 W); (f) the variation in the temperatures of sample surface with the RF powers, and the inset is the thermal image under 620 W of RF power.

this study is single crystal silicon. (100) is the crystal plane parallel to the wafer surface. The size of wafers was 10 mm × 10 mm × 0.5 mm and the diameter of ICP irradiated region was 20 mm, thus the temperature in the irradiated region under the plasma torch was recorded as the surface temperature. When the RF power was 620 W, the average temperature of the Si wafer surface was 920.7 °C. The research also shows that the surface temperature has a linear relationship with RF power, as shown in Fig. 2(f). By adjusting the power, the surface temperature of Si wafer surface can be roughly controlled from 400 to 1100 °C.

The compositions of free radicals of ICP in the plasma-OX and plasma-AMM processes were detected by an optical emission spectrometer (OES, Ocean Optics USB4000) with a wavelength resolution of 0.2 nm. As seen in Fig. 2(b), the fiber optic probe was fixed at a distance of about 200 mm from the torch center, and the spectral information of all collected data was recorded with a constant integration time of 60 ms. The wavelength of the emission spectrum can be used to deduce its energy, and then the composition of the transition group can be calibrated. The emission intensity reflects the density of free radicals to some extent.

The parameters in plasma-OX and subsequent plasma-AMM processes are shown in Table 1. In the plasma-OX process (RF 500 W), argon was used as the ignition gas (Ar, 1.5 slm). Corresponding to the deexcitation of argon atoms, some strong argon peaks (751.5 nm, 763.5 nm, 811.5 nm, 842.5 nm, etc.) were observed [44,45], as shown in Fig. 2(c). Due to the introduction of a large amount of oxygen, two distinct strong oxygen peaks (671.4 nm and 772.9 nm) were observed corresponding to the deexcitation of the oxygen atom. Compared to the OES spectra in plasma-OX process, the intensity of two oxygen peaks (671.4 nm and 772.9 nm) were weakened in plasma-AMM process (RF power 620 W) while others were almost same, shown in Fig. 2(d).

In order to better characterize the interface morphology, the silicon oxide film on the surface of Si wafers need to be removed. Hydrofluoric acid (HF) was used to remove silicon oxide film efficiently [46,47], which is based on the reaction of HF and SiO_2. The chemical reaction of oxide film and HF can be expressed as Eq. (3) [48]:

$$SiO_{2(solid)} + HF_{(aq)} + H^{+} \rightarrow SiF_6^{2-}{}_{(aq)} + H_2O_{(aq)} \quad (1)$$

To realize a stable etching of silicon oxide film, NH_4F solution was added to HF solution, which was called buffered oxide etch (BOE) solution [49]. Thus, the processed Si wafers were placed in the BOE solution for 10 min. The reaction diagram of oxide film in BOE solution is shown in Fig. 3. The processed Si wafers were placed in the BOE solution for 10 min. The EDS (Energy Dispersive Spectrometer) spectrum was used to analyze the contents of the main elements of surface, as shown in Fig. S1. It indicates that the silicon oxide film can be removed in 10 min etching.

Table 1
The Plasma-OX and the subsequent plasma-AMM process parameters.

Parameters	Plasma-OX	Plasma-AMM
Ignition gas (Ar)	1.5 slm	
Cooling gas (Ar)	18.0 slm	
O_2	60 sccm	0
Frequency	27.12 MHz	
RF power	500 W	560–700 W
Distance	10 cm	
Time	2 min	5 min

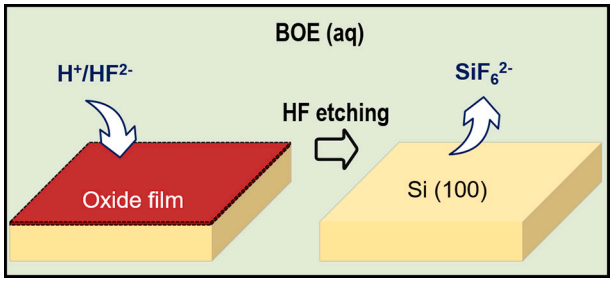

Fig. 3. Schematic diagrams of HF etching with oxide layer on the Si surface.

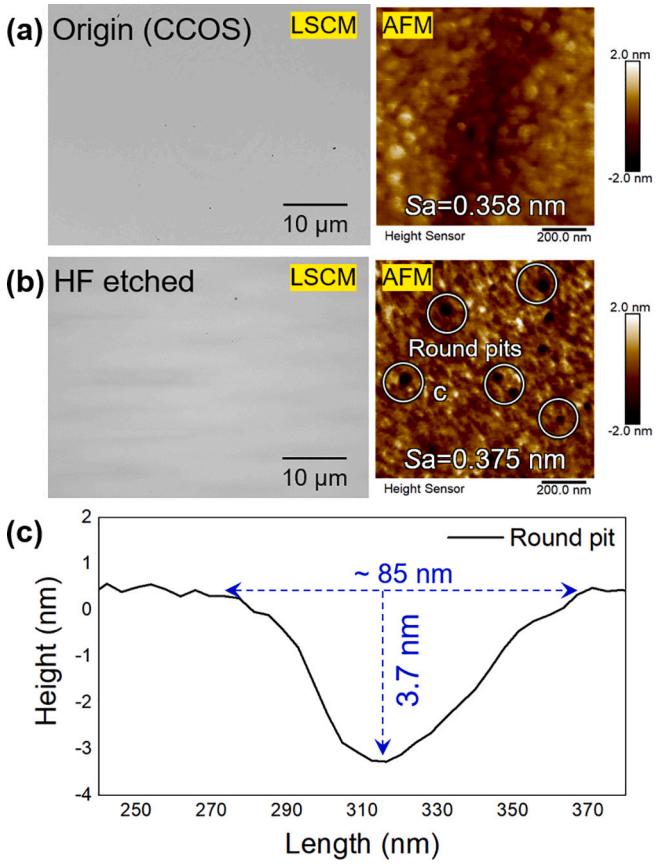

Fig. 4. LSCM and AFM images: (a) Origin surface, (b) The exposed surface after HF etching 10 min; (c) The profiles of regular-round-pits of AFM images in (b).

The Si wafer by computer controlled optical surfacing (CCOS) manufacturing is widely used in commercial sales due to the smooth surface with less subsurface damage. Thus, the original states of *c*-Si (100) wafer processed by CCOS were studied as original samples. All wafers were ultrasonically cleaned with high purity alcohol (99.5 %) and rinsed in ultra-pure water, then dried with nitrogen (99.999 %). The surface morphology was observed by laser scanning confocal microscope (LSCM, Keyence VK-X1000), and the surface roughness was measured by atomic force microscope (AFM, Bruker Edge). For the purpose to clarify the structural evolution of the subsurface processed by plasma-OX and OX-AMM hybrid processes, the lamellar specimens for high resolution transmission electron microscope (HRTEM) analysis were lifted out by a dual-beam scanning electron microscopy/focused ion beam (SEM/FIB) system. The X-ray diffraction (XRD) data were obtained by a Philips 60 X'Pert PRO powder diffractometer using Cu Kα radiation (λ 1.54055 Å) at 40 kV and 10 mA. The incident beam was passed through an X-ray mirror having a divergence slit of 1/2. The diffracted beam was directed to the detector through a parallel plate collimator with equatorial acceptance slit of 1/4.

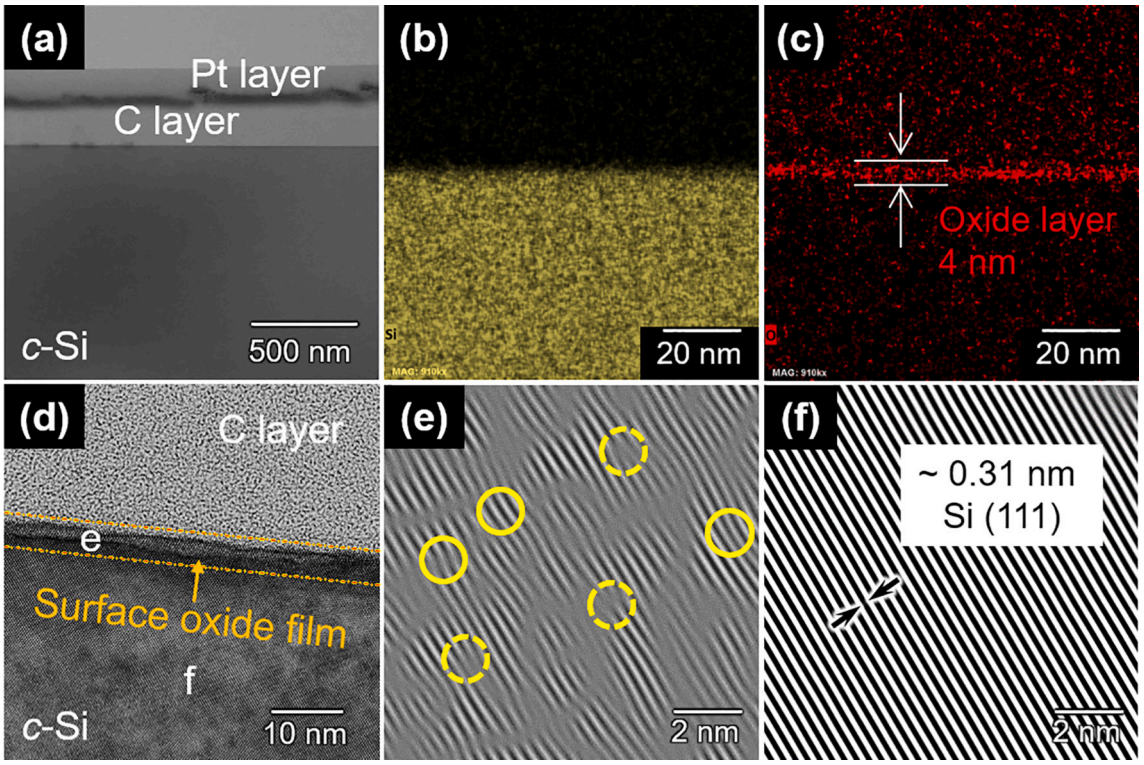

Fig. 5. The subsurface characteristics of the original Si wafer: (a) HRTEM image of the whole subsurface at hundreds nanoscale; EDS images of the silica element (b) and oxygen elements (c); (d) HRTEM image of the surface oxide film at tens nanoscale; Lattice fringe images of interface (e) and *c*-Si (f). The solid yellow circles represent the twisted lattice and the dashed yellow circles represent dislocations. (For interpretation of the references to color in this figure legend, the reader is referred to the web version of this article.)

3. Results

3.1. The original surface/subsurface of Si

The morphology of original surface/subsurface was observed firstly. Fig. 4(a) shows the original morphologies of Si surface by LSCM and AFM images. The original surface was smooth and the roughness was *Sa* 0.358 nm. HF etching was used to remove oxide film and exposed surface morphology is shown in Fig. 4(b). After HF etching, the surface was also smooth and the roughness was *Sa* 0.375 nm, which was near the original surface due to the re-natural oxidation of the Si wafer surface in atmospheric environment. The several tens nanoscale round-pits are observed in the AFM image, as shown in Fig. 4(b). HF reacted with Si oxides and completed etching quickly, but reacted with *c*-Si slowly. Therefore, these round-pits exposed after HF etching were presumed to be derived from nanoscale subsurface defects on the original surface processed by CCOS. The higher oxygen content at these subsurface defects provided HF adsorption with more active sites. As shown in Fig. 4 (c), the surface profiles exhibit the nanoscale depth of these round-pit, which confirmed the CCOS processed surface of Si wafer was to some extent smooth with less damage at nanoscale.

Fig. 5 shows the subsurface characteristics of the original Si wafers. The HRTEM image of the whole surface at hundreds nanoscale is shown in Fig. 5(a). The carbon layer covered on the wafer surface was used to avoid damage of oxide film during FIB process. The EDS (Si) and EDS (O) distribution mappings of the cross-section for the unprocessed original surface are shown in Fig. 5(b) and (c). The thickness for high-content oxygen region of was about 4 nm, which was caused by the previous step processing procedure, i.e., natural oxidation. Fig. 5(d) shows the HRTEM image for the original Si surface at tens nanoscale. An obvious oxide film was observed on the surface, with thickness at nanoscale. However, the oxide film was not completely orderly as indicated by the yellow dotted line. On the contrary, the atoms in *c*-Si are arranged in order, so the arrangement of atoms in the oxide film and *c*-Si is further observed.

The lattice fringes of *c*-Si were uniform and clear, shown in the Fig. 5 (e). Meanwhile, the lattice fringe spacing was about 0.31 nm, corresponding Si (111). The high-resolution images obtained by TEM came from the cross section of the surface material. The lattice fringes for (111) plane was original from the electron diffraction images and FFT/IFFT calculation, which was in connection with the relationship of the crystallographic zone axis and the direction of the transmitted electron beam.

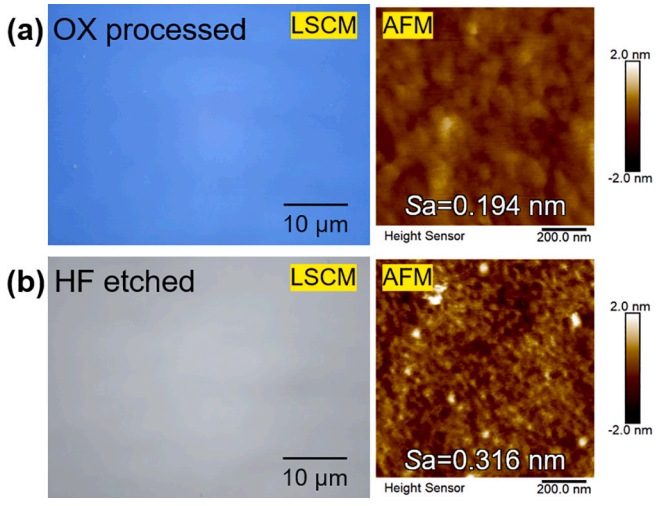

Fig. 6. LSCM and AFM images: (a) Plasma-OX processed surface, (b) The exposed interface after HF etching.

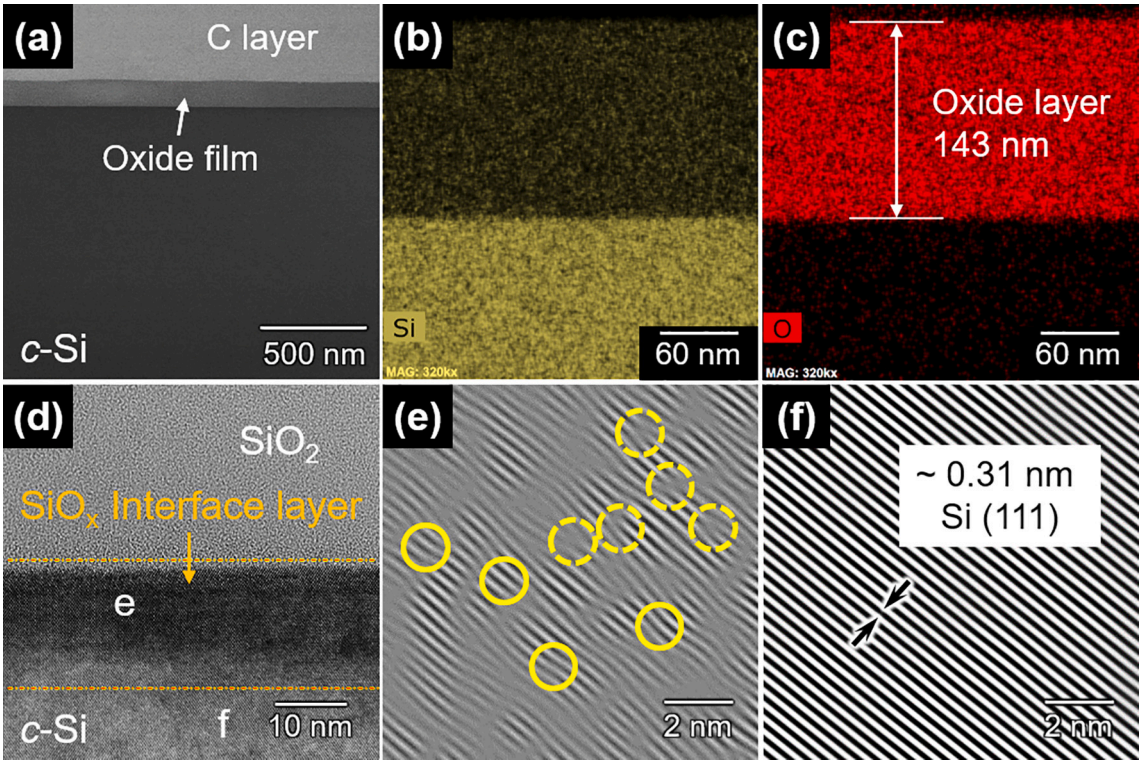

Fig. 7. The subsurface characteristics of the OX processed Si wafer: (a) HRTEM image of the whole subsurface at hundreds nanoscale; EDS images of the silica element (b) and oxygen elements (c); (d) HRTEM image of the SiO_2/Si interface at tens nanoscale; Lattice fringe images of interface (e) and *c*-Si (f).

The dislocations and lattice distortions can be identified in the lattice fringe in oxide film, shown in the Fig. 5(e). As interstitial atoms, the doped oxygen atoms caused defects in *c*-Si, which destroyed the equilibrium state between Si atoms and distorted the lattice. Therefore, the lattice distortions were observed on the surface, as marked by solid circles. Meanwhile, the lattice distortions formed local slip in the crystal structure, which led the generation of edge dislocations, as marked by dotted circles. The thermal stress is another major factor in generating lattice distortion and edge dislocations. The doping of oxygen atoms in the natural oxidation process was conducted in normal temperature and pressure environment, thus the lattice distortion and edge dislocation were derived from the doping of a small amount of oxygen atoms in the natural oxidation process. However, the subsurface defects of the CCOS processed original wafer easily adsorbed oxygen atoms, which led the observable dislocations and lattice distortions. The original oxide film on the Si surface was considered as SiO_x ($x < 2$), consisting of *c*-Si and doping O atoms, which was consistent with previous speculation.

3.2. The OX processed interface SiO_2/Si

The plasma-OX process was first conducted on the original surface of Si wafer as the first step. The RF power is 500 W, and the corresponding wafer surface temperature was maintained at about 751.2 °C, shown in Fig. 2(f). Based on short-term and thermal oxidation, the oxide film on the Si surface became thickened rapidly in plasma-OX process. Fig. 6(a) shows the surface morphology of the plasma-OX processed oxide film by LSCM and AFM images. The color of LSCM image is significant light blue, and the surface roughness in the AFM image is *Sa* 0.194 nm. After HF etching 10 min, the oxide film was removed and the exposed morphology of SiO_2/Si interface is shown in Fig. 6(b). Compared with the original surface morphology (Fig. 4(b)), the round pits on the original surface disappeared observing from the AFM image, which was due to the depth of oxidation exceeded that of the round pits.

The subsurface characteristics of the OX processed Si wafers is shown in Fig. 7. The HRTEM image for the whole surface characteristics at hundreds nanoscale is shown in Fig. 5(a) and a significant oxide film on the surface was observed. The EDS (Si) and EDS (O) distribution mappings of the cross-section for the plasma-OX processed surface are shown in Fig. 7(b) and (c). The thickness for high-content oxygen region of was about 143 nm, which was caused by the thermal oxidation procedure. According to the analysis of the bonding mechanism of Fig. 1 (a), oxygen cannot be completely matched up with silicon due to excessive oxygen injection and short-term oxidation treatment, so the oxide layer is composed of SiO_2 layer and SiO_x ($x < 2$) layer. Fig. 7(d) shows the HRTEM image for the SiO_2/Si interface characteristics at tens nanoscale, in which the SiO_2 layer is on the top, the *c*-Si region is at the bottom, and a transitional SiO_x layer in the middle. The structure for SiO_x layer is similar to that for *c*-Si, but the structure was blurred, and there are some obvious dislocations and distortions as indicated by the yellow line.

In order to observe and compare the atomic arrangement on the SiO_2/Si interface, the lattice fringe images are shown in Fig. 7(e) and (f). Severe lattice distortions and edge dislocations can be observed on the lattice fringe of SiO_x layer, as marked by yellow circles. Compared with the original surface, the density of distortion in the SiO_x layer was larger and the degree of lattice deformation was more serious. A large number of oxygen atoms infiltrated on the wafer surface, forming a serious doping phenomenon. Meanwhile, the high temperature oxidation also promoted the oxygen doping and residual thermal stress, which caused serious lattice defect. The excess oxygen atoms seriously destroyed the crystal structure, leaving a certain amount of free Si atoms, which provided the premise of Si atom migration in the next-step process.

3.3. The OX-AMM processed interface SiO_2/Si

Plasma-OX prepared a thick oxide film on the Si wafer surface, and the subsequent plasma-AMM was used as the second processing

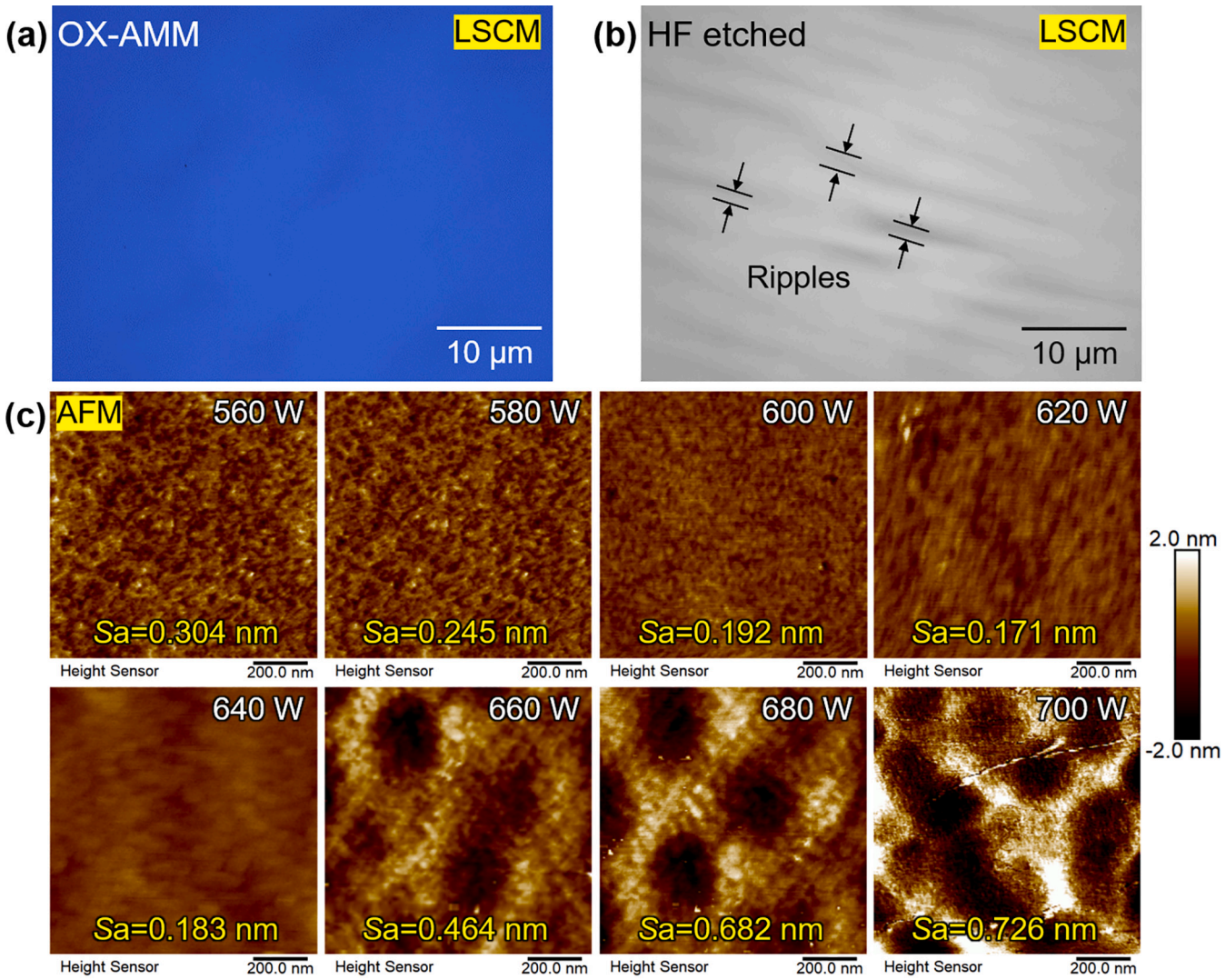

Fig. 8. (a) The LSCM image of the OX-AMM processed Si wfer surface; (b) Exposed SiO_2/*c*-Si interface after HF etching 10 min; (c) AFM images of SiO_2/*c*-Si interface at different AMM powers.

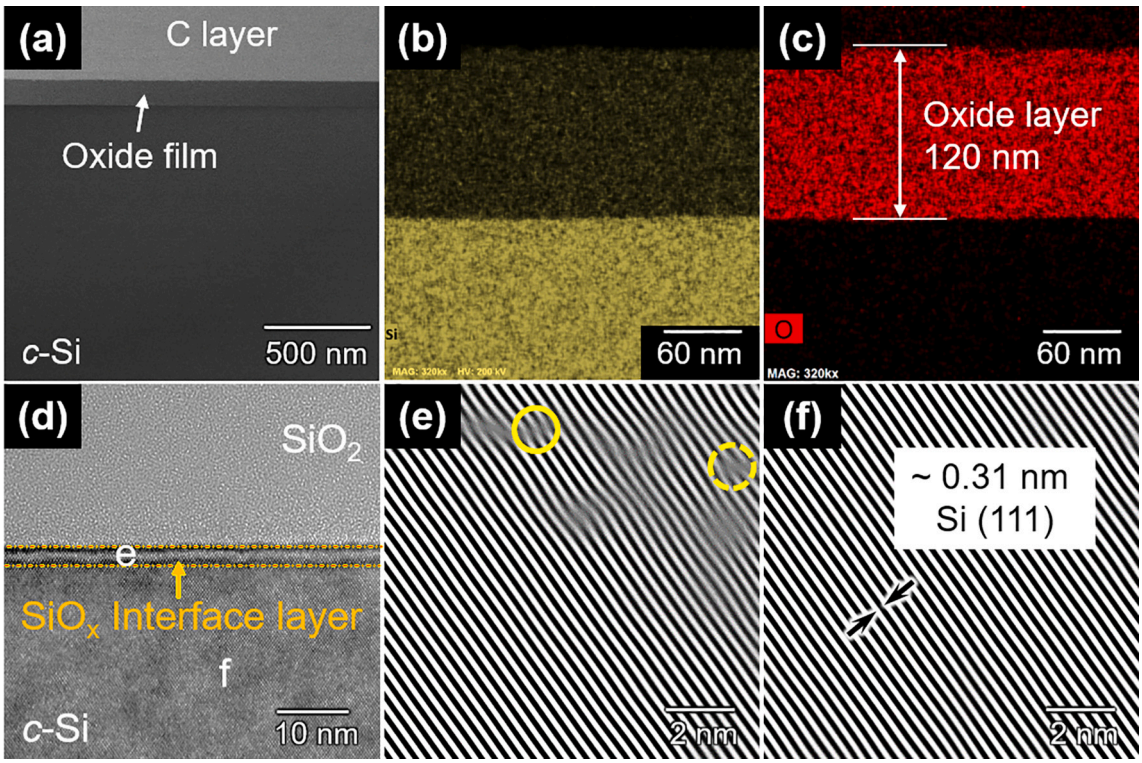

Fig. 9. The subsurface characteristics of Si wafer processed by the OX-AMM (620 W): (a) HRTEM image of the subsurface at hundreds nanoscale; EDS images of (b) the silica element and (c) oxygen element; (d) HRTEM image of the SiO_2/Si interface at tens nanoscale; lattice fringe images of (e) the interface and (f) *c*-Si.

procedure. Fig. 8(a) shows the subsequent AMM processed surface of LSCM image, in which the color is blue. Fig. 8(b) displays the exposed SiO_2/Si interface after HF etching observing by LSCM, and some microscale ripples were identified. It can be inferred that the plasma induced the atoms migration of Si wafer under the high-temperature, and it realized the softening of the SiO_x interface layer in AMM process. As AMM process was stopped, there was a sharp heat exchange between wafer surface of high temperature and the atmosphere of normal temperature. Thus, these microscale ripples in the SiO_2/Si interface may be resulted from the rapid cooling.

With respect to plasma-AMM process, the power was the main factor for the migration efficient of atoms [41,42]. The plasma-AMM experiments of various powers were conducted in Fig. 2(f). For exploring the effect of RF power on the interface morphology, Fig. 8(c) shows the exposed SiO_2/Si interface by AFM images at different plasma-AMM powers. The corner areas of Si wafer begin to melt when the power exceeded 700 W, which affected the surface structure seriously. Therefore, the power used in the plasma-AMM process was <700 W. When the power was set as 560 W, there was little change in the exposed morphology and roughness of SiO_2/Si interface, compared with the plasma-OX processed interface. When the power increased, the roughness of the SiO_2/Si interface gradually decreased to the lowest value of *S*a 0.171 nm at AMM 620 W. As for further increasing the power during AMM process, the roughness of the surface began to deteriorate, and the highest value of *S*a reached to 0.726 nm at AMM 700 W. At higher AMM powers, the island structures were formed. Thus, 620 W in the plasma-AMM was the most suitable process parameters. However, the rapid cooling may be the key factor for generating microscale ripples of the surface. Owning to the micro-melting of the SiO_x interface layer under excessive power, the rapid cooling of the SiO_x interface layer led to the island structures. In order to eliminate the microscale ripples morphology, the optimization of plasma-AMM process was necessary so as to manufacture a flatting SiO_2/Si interface.

The HRTEM image for the surface characteristics of the OX-AMM (620 W) processed Si wafers is shown in Fig. 9 (a). The EDS (Si) and EDS (O) distribution mappings of the cross-section for the OX-AMM processed surface are shown in Fig. 9(b) and (c). The thickness for high-content oxygen region of was reduced to ~120 nm. The HRTEM image for the SiO_2/Si interface is shown in Fig. 9(d), and the thickness of the interface is at several nanoscales and apparently less than that of the interface processed only by OX plasma process. It was in line with the analysis of the migration mechanism of Fig. 1(b), which is the speculation of decomposition of SiO_x layer and the Si re-bonding to *c*-Si.

The lattice fringe image of SiO_x layer is shown in Fig. 9(e), and the *c*-Si lattice fringes can be observed on most of the SiO_x interface layer. Compared with the plasma-OX processed SiO_x interface defects, the density of lattice distortion was decreased and the lattice deformation almost disappeared. The ICP only carried argon without oxygen. On the one hand, the energy transferred into the SiO_x interface continuously, thus Si atoms in the SiO_x layer migrated and boned to *c*-Si, which realized the thinning of SiO_2/Si interface and removed defects. On the other hand, the oxide film hindered the oxygen atoms in the atmospheric environment from permeating the interface, which avoided the new doping. However, the OX-AMM processed SiO_x layer was still recognized, and its thickness was 2–3 nm. A small number of residual defects were derived from the residual thermal stress after the plasma-AMM process due to the rapid cooling. In order to completely eliminate residual defects and reduce the thickness of SiO_2/Si as much as possible, the plasma-AMM process needs to be optimized.

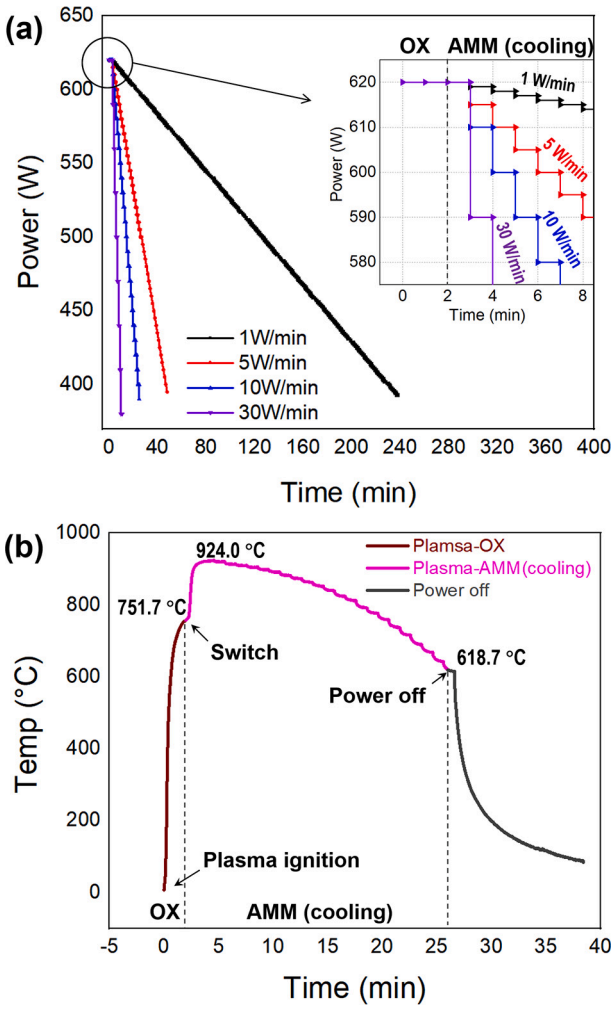

Fig. 10. The OX-AMM process with cooling settings, (a) the relationships of the setting RF powers and time under different cooling rates; (b) the change of temperature with time for sample from the beginning of manufacturing to the ending of the cooling process (10 W/min) and natural cooling.

3.4. The OX-AMM (cooling) processed interface SiO_2/Si

It is likely that the rapid cooling results in the streamlined morphography and residual defects of the SiOx layer. Thus, the core of optimizing plasma-AMM was to realize multi-steps slow cooling at a constant power. The minimum roughness of plasma-AMM process in constant power was obtained at 620 W, thus 620 W was used for the initial power. The power decreased from 620 W to below 400 W at the different rates in the plasma-AMM (cooling) process. Fig. 10 (a) shows the powers value versus time at the different cooling rates. The decreasing trend of RF power is approximately in linear, and the inset image shows the enlarged graph relation of time and setting power. The decreased value for each step is in the fixed power and the setting power maintained for one minute in each step. For directly elucidating the variation of temperature of sample and time, the curve of temperature and time in the whole process was recorded when the cooling setting of RF power is 10 W/min, as shown in Fig. 10(b). In plasma-OX process, the temperature of wafer surface increased from room temperature to 751.7 °C in 2 min. By switching to plasma-AMM process, temperature of wafer surface increased to 924.0 °C subsequently. The setting cooling procedure can control the temperature of the wafer surface decreasing from 924.0 °C to 618.7 °C in 25 min, which is different from rapid cooling after plasma-AMM. Then, the power was off and the temperature was decreased rapidly.

Fig. 11 (a) shows the surface morphology of sample processed after OX-AMM (cooling) observed by LSCM under 10 W/min of cooling RF power, which was similar to that after OX-AMM processing. Fig. 11(b) shows the exposed SiO2/Si interface morphology after HF etching. It is worth noting that there were no ripples observed on the smooth SiO_2/Si interface, which is different from the surface condition after OX-AMM process without cooling processing. It means that multi-step slow cooling mode can reduce the influence of thermal stress.

Fig. 11(c) shows the AFM topography of the exposed SiO2/Si interface after etching, which were OX-AMM processed at different cooling rates. When the cooling rate was 30 W/min, the roughness of SiO2/Si interface was decreased to 0.116 nm significantly. Besides, when the cooling rate decreased to 10 W/min, the roughness of Sa can decrease to 0.0842 nm. With respect to these lower cooling rate of 5 W/min and 1 W/min, the roughness for the SiO2/Si interface cannot be reduced obviously, and it is stabilized at 0.08–0.09 nm. The results confirm that the ultra-smooth SiO2/Si interface can be processed through the multi-step slow cooling process, which can reduce the microscale ripples and nanoscale streamlined morphology. The optimized plasma-AMM (cooling) process can make a breakthrough in manufacturing ultra-smooth surface with its roughness of Sa below 0.1 nm. Fig. 11(d) shows the HRTEM image for the SiO_2/Si interface characteristics of the OX-AMM (cooling) processed wafer at tens nanoscale. A significant flatting SiO_2/Si interface was observed, and the SiO_x layer thickness is below 0.6 nm (1–2 atoms layer). The lattice fringe image of SiO_2/Si interface is shown in Fig. 11(e) and *c*-Si is shown in Fig. 11(f). Compared with the OX-AMM processed SiO_x interface, the lattice distortion and deformation completely disappeared. The lattice fringe image in the SiO_2/Si interface was same to *c*-Si, and there is not observed dislocation morphology. Thus, it can be considered that the SiO_x completely decomposed and disappeared, and the atomic-level ultra-smooth and ultra-thin SiO_2/Si interface was processed.

4. Discussion

A thick oxide film was formed on the surface of the Si wafer after the plasma-OX process, including an oxygen-saturated layer (SiO_2) on the top and a significant oxygen-unsaturated layer (SiO_x, $x < 2$) adjacent to the bulk crystal silica (*c*-Si). After the subsequent plasma-AMM process, the Si atoms in the SiO_x layer migrated and re-bonded to *c*-Si, and the SiO_x layer became thinner. Based on the OX-AMM hybrid process, the SiO_x layer gradually decomposed and a smooth and thin SiO_2/Si interface on the subsurface was formed. By optimizing the OX-AMM (cooling) process, the thickness of SiO_x layer between SiO_2 the *c*-Si can reduce to <0.6 nm, with surface roughness of *Sa* < 0.1 nm. Fig. 12(a) shows the HRTEM images at nanoscale for the interface characteristics after different processed Si wafers, and Fig. 12 (b) shows the corresponding lattice fringe images.

On the original Si wafer surface, the interface atomic arrangement neighboring *c*-Si is blurred due to the doping oxygen atoms in nature oxidation process. Thus, the slightly distorted and curved lattice fringes are observed in the SiO_x layer of original Si surface. On the plasma-OX processed Si wafer surface, the interface atomic arrangement neighboring *c*-Si is more irregular due to the excessive doping oxygen atoms and thermal stress in the thermal oxidation process. Thus, severe distorted and curved lattice fringes can be observed in the SiO_x layer of plasma-OX processed Si surface. On the OX-AMM processed Si wafer surface, the interface atomic arrangement neighboring *c*-Si is clear. Because of the stably transferring energy, the free Si atoms in the SiO_x layer migrated and bonded to the *c*-Si. This process led the decomposition of SiO_x layer and the defects are eliminated. Without new doping oxygen atoms, there was no new defects from doping on the SiO_2/Si interface. However, the rapid cooling after the plasma-AMM still brings thermal stress, leading a small number of residual defects. Thus, slight fuzzy fringes were observed in the SiO_x layer of OX-AMM processed Si surface. In order to completely eliminate the influence of thermal stress,

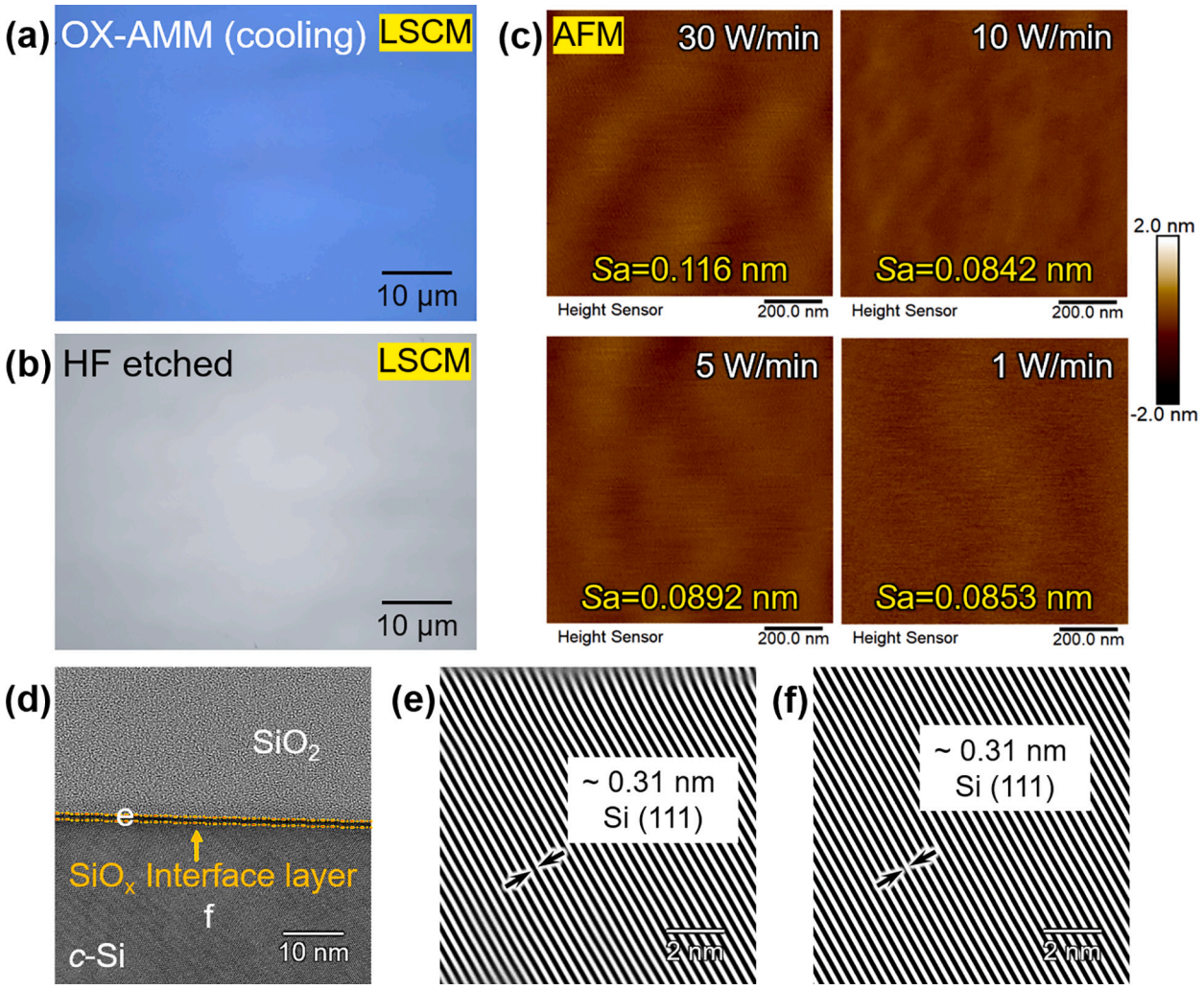

Fig. 11. The LSCM images of (a) the OX-AMM (cooling) processed Si surface and (b) the exposed SiO_2/c-Si interface after HF etching; (c) AFM images of the exposed SiO_2/Si interfaces at different cooling rates; (d) HRTEM image of SiO_2/Si interface, (e) lattice fringe image of SiO_2/Si interface and (f) c-Si after the plasma-AMM (cooling) process at cooling rate of 10 W/min.

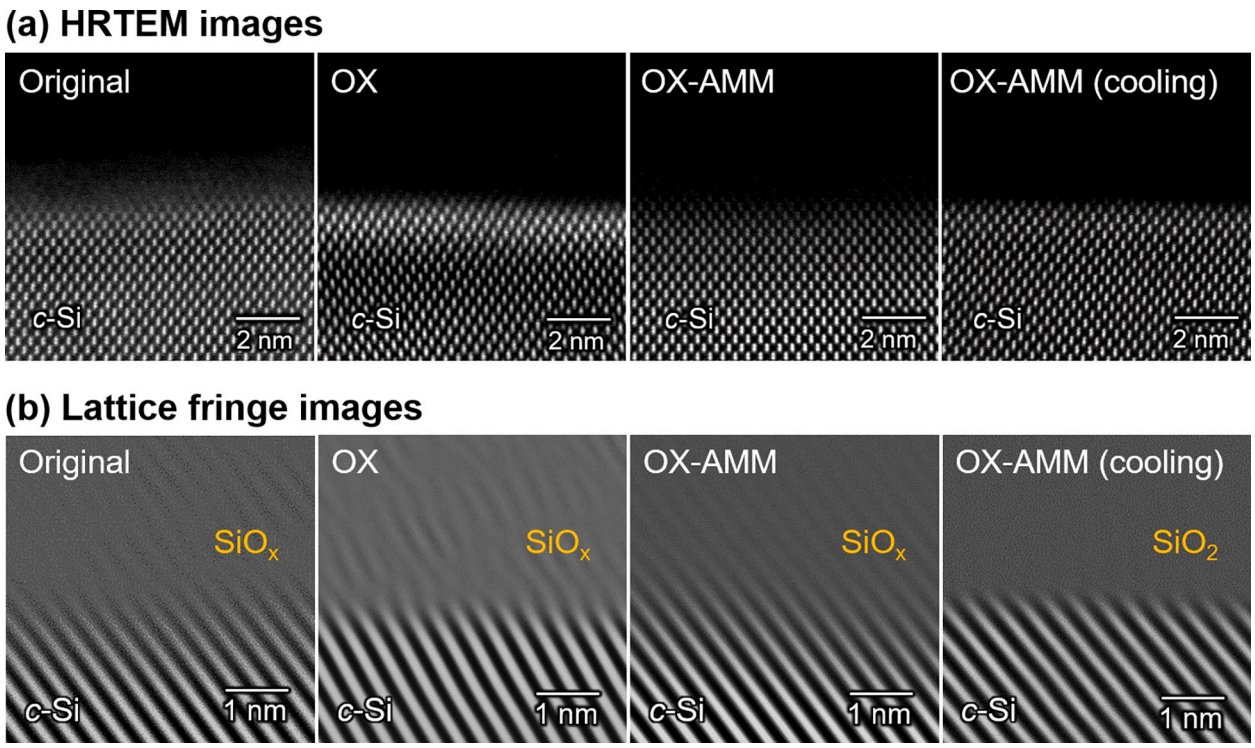

Fig. 12. (a) The HRTEM images and (b) lattice fringe images for the characteristics of SiO_2/Si interface neighboring *c*-Si region of the Si wafers surface after different processes at nanoscale.

multi-step slow cooling is designed in plasma-AMM. On the OX-AMM (cooling) processed Si wafer surface, the interface atomic arrangement neighboring *c*-Si was extremely clear. By stably transferring energy in multi-step slow cooling mode, the plasma-AMM (cooling) process can avoid the thermal stress to a great extent. Thus, a significant amorphous region and lattice fringes region were observed SiO_2/Si interface of OX-AMM (cooling) processed Si surface, and an ultra-thin SiO_2/Si interface can be processed.

As the final procedure, HF etching is used to remove the oxide film and expose the interface morphologies. Fig. 13(a) shows the exposed profiles and roughness values of the original surface and the SiO_2/Si interfaces after different processes from AFM images in Figs. 4(b), 6(b), 8(d) and 11(c). The original surface was composed of SiO_x layer, and the roughness was Rq 1.42 nm and Ra 0.257 nm. After thermal oxidation of plasma-OX process, the SiO_2/Si interface is mainly composed of SiO_x layer. Therefore, the plasma-OX processed roughness of SiO_2/Si interface was Rq 1.62 nm and Ra 0.247 nm, which was similar to original surface. The subsequent plasma-AMM process thinned the thickness of SiO_x layer to 2–3 nm, and the SiO_2/Si interface was flatting. Thus, the exposed SiO_2/Si interface after HF etching was smooth, with the roughness reduced to Rq 1.07 nm and Ra from 0.161 nm. By optimizing plasma-AMM (cooling) process, the thickness of SiO_x layer can decrease to below 0.6 nm and the roughness of exposed SiO_2/Si interface is Rq 0.421 nm and Ra < 0.1 nm.

For further elucidating the morphology evolution of the Si wafers, the power spectral density (PSD) analysis was conducted on the data from AFM images of the SiO2/Si interface. Data fitting of PSD is shown in Fig. 13(b). It is evident that interface roughness within measured range of high spatial frequency is effectively decreased during OX-AMM and OX-AMM (cooling) processes.

Furthermore, the interfacial roughness is obtained by removing the surface oxide film by HF etching. Therefore, it is necessary to detect the surface after HF etching to determine the crystal orientation and element distribution of the surface. Fig. 14 shows the XRD spectra of the original wafer and HF etched wafer surfaces. All the spectrums show individual peak in almost the same position of Si (311) orientation, which confirmed HF etching did not change the crystal orientation of the wafer surface.

The asymmetric characteristic at the bottom of the diffraction peak on the original surface can be understood as the oxygen doping by natural oxidation and the original subsurface damage. After HF etching, a natural oxide film was formed on the surface again, and the diffraction peak of the film was almost unchanged. The thermal oxidation process included excessive oxygen doping and thermal stress, which led to the obvious left shift of diffraction peak. Further the plasma-AMM process releases the stress at the interface and the diffraction peak returns to the right. After the optimized plasma-AMM (cooling) tuning, the stress was almost completely released and the diffraction peak returned to the initial position. Moreover, the intensity of diffraction peak increased significantly and the full width at half maxima (FWHM) decreased after AMM (cooling) tuning, which confirms that the materials on the surface became excellent crystallization.

5. Conclusion

This study proposed an efficiently process for ultra-flat and ultra-thin SiO_2/Si interface by combining plasma-OX process and plasma-AMM process. By optimizing process, the roughness and thickness of SiO_x/Si interface can be rapidly reduced to atomic level. The proposed OX-AMM hybrid process was conducted on one ICP setup by adjusting the airflow. The conclusion is as follows:

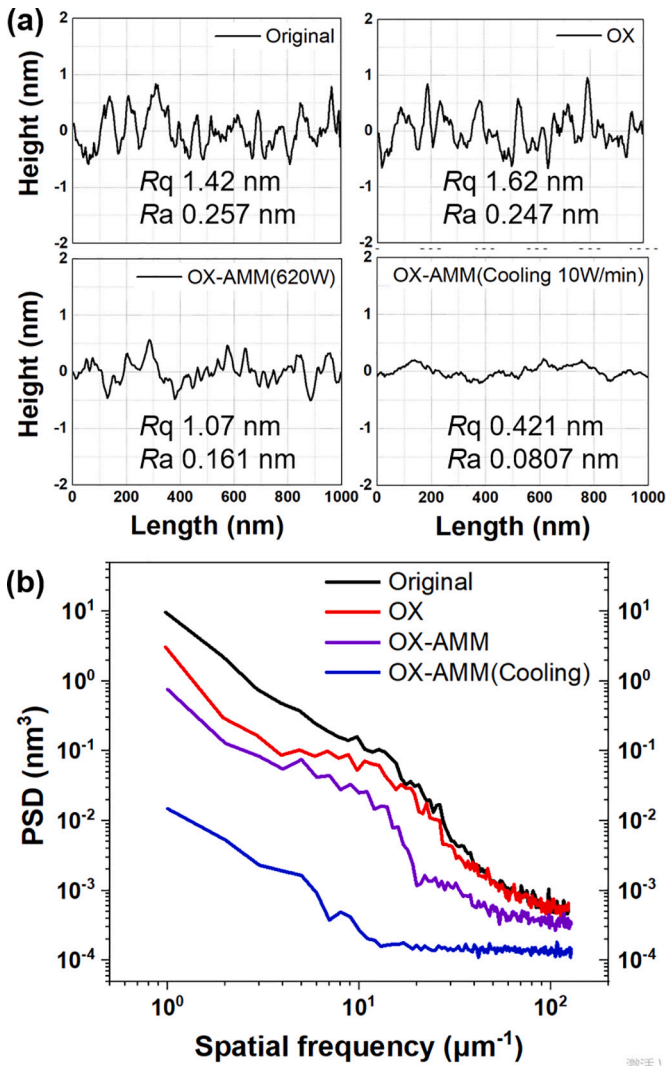

Fig. 13. (a) The surface profiles (by AFM, 1 μm × 1 μm) of HF etched Si wafers at different processes; (b) The PSD curves of the SiO_2/Si interface after HF etching at different processes.

(1). The oxide film thickness of original Si surface was 0.4 nm. The atomic arrangement of surface was blurred with same dislocation defects, with the roughness *Sa* 0.375 nm.

(2). In the ICP oxidization mode, the plasma-OX process overlaid an oxide film with thickness 140 nm on the *c*-Si surface in 2 min, which formed a SiO_2 layer on the top and a SiO_x ($x < 2$) layer neighboring to *c*-Si. Compared with the original sample, the atomic arrangement of SiO_2/Si interface was not improved, and the roughness was *Sa* 0.316 nm.

(3). In the ICP migration mode, the plasma-AMM process induced Si atoms migration to *c*-Si and the SiO_x layer gradually decomposed in 5 min. At 620 W RF power, the thickness of oxide film was reduced to 120 nm and the thickness SiO_x layer was reduce to about 2–3 nm. The roughness of SiO_2/Si interface was reduced to *Sa* < 0.2 nm. In comparison, traditional thermal annealing consumed hours to achieve atomic-level interface

(4). By optimizing multi-step cooling plasma-AMM tuning, the SiO_x layer was almost completely decomposed with thickness of 1–2 atom layers and the interface defects was completely removed. While annealing rate was set as 10 W/min, the SiO_2/Si interface roughness achieved *Sa* < 0.1 nm, which was close to physical limit.

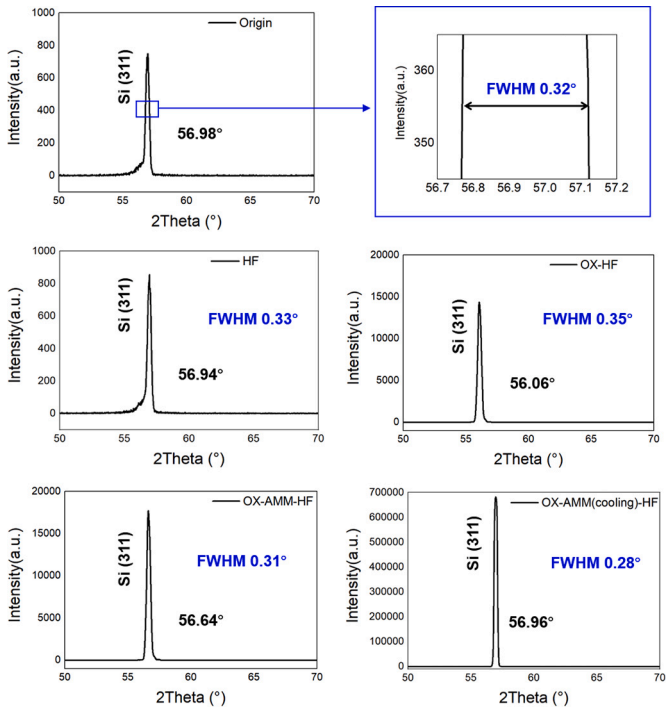

Fig. 14. XRD spectrums of original surface and HF etched surface of different processed stages.

(5). This plasma-induce OX-AMM hybrid process provides a potential manufacturing method for SiO_2/Si interface applied in MOSFET. It also shows a possibility for ultra-smooth Si surface by HF etching as the final process to remove the SiO_2 oxide film, which may be further extended for manufacturing Si semiconductor devices.

Declaration of competing interest

The authors declare that they have no known competing financial interests or personal relationships that could have appeared to influence the work reported in this paper.

Acknowledgements

This project is supported by the National Natural Science Foundation of China (52035009), the Natural Science Foundation of Guangdong Province (2023A1515011461) and the Science and Technology Innovation Committee of Shenzhen Municipality (JCYJ2022081810041 2027). The authors acknowledge the assistance of SUSTech Core Research Facilities.

Appendix A. Supplementary data

Supplementary data to this article can be found online at https://doi.org/10.1016/j.jmapro.2023.10.045.

References

[1] Kathiravan S, Kaliaraj GS, Kumar RR, Kirubaharan AK. A novel experimental setup for in situ oxidation behavior study of Nb/Hf/Ti (C-103) alloy for high temperature environments. Mater Lett 2021;302:130336.
[2] Pan S, Yao G, Guan Z, Yu N, Sokoluk M, Li X. Kinetics and dynamics of surface thermal oxidation in Al-ZrB_2 nanocomposites. Corros Sci 2020;176:108890.
[3] Liu C, Zhang Y-M, Zhang Y-M, Lü H-L. Interfacial characteristics of Al/Al2O3/ZnO/n-GaAs MOS capacitor. Chin Phys B 2013;22:076701.
[4] Suzer S, Sayan S, Banaszak Holl M, Garfunkel E, Hussain Z, Hamdan N. Soft x-ray photoemission studies of Hf oxidation. J Vac Sci Technol A 2003;21:106–9.

[5] Gaburro Z, Pucker G, Bellutti P, Pavesi L. Electroluminescence in MOS structures with Si/SiO_2 nanometric multilayers. Solid State Commun 2000;114:33–7.
[6] Zheng T, Li Z. The present status of Si/SiO_2 superlattice research into optoelectronic applications. Superlatt Microstruct 2005;37:227–47.
[7] Sasada T, Nakakita Y, Takenaka M, Takagi S. Surface orientation dependence of interface properties of GeO2/Ge metal-oxide-semiconductor structures fabricated by thermal oxidation. J Appl Phys 2009;106.
[8] Sun J, Lu J. Interface engineering and gate dielectric engineering for high performance Ge MOSFETs. Adv Condens Matter Phys 2015;2015.
[9] Ernst F. Metal-oxide interfaces. Mater Sci Eng R Rep 1995;14:97–156.
[10] Loh T-H, Wang Q, Ng K-T, Lai Y-C, Ho S-T. CMOS compatible integration of Si/SiO_2 multilayer GRIN lens optical mode size converter to Si wire waveguide. Opt Express 2012;20:14769–78.
[11] Takenaka H, Hatayama M, Ito H, Ohchi T, Takano A, Kurosawa S, et al. Development of Si/SiO_2 multilayer type AFM tip characterizers. J Surf Anal 2011; 17:264–8.
[12] Pantelides ST, Wang S, Franceschetti A, Buczko R, Di Ventra M, Rashkeev SN, et al. Si/SiO_2 and SiC/SiO_2 interfaces for MOSFETs – challenges and advances. In: Materials science forum; 2006.
[13] Inoue F, Podpod A, Peng L, Phommahaxay A, Rebibis KJ, Uedono A, et al. Morphological characterization and mechanical behavior by dicing and thinning on direct bonded Si wafer. J Manuf Process 2020;58:811–8.
[14] Pease RF, Chou SY. Lithography and other patterning techniques for future electronics. Proc IEEE 2008;96:248–70.
[15] Culcer D, Hu X, Sarma SD. Interface roughness, valley-orbit coupling, and valley manipulation in quantum dots. Phys Rev B 2010;82:205315.
[16] Goswami S, Slinker K, Friesen M, McGuire L, Truitt J, Tahan C, et al. Controllable valley splitting in silicon quantum devices. Nat Phys 2007;3:41–5.
[17] Xie W, Zhang Z, Wang L, Cui X, Yu S, Su H, et al. Chemical mechanical polishing of silicon wafers using developed uniformly dispersed colloidal silica in slurry. J Manuf Process 2023;90:196–203.
[18] Liu X, Wang B, Li Y, Zhou Y, Zhang J, Wang Z, et al. Improving machinability of single-crystal silicon by cold plasma jet. J Manuf Process 2023;99:581–91.
[19] Fang F. The three paradigms of manufacturing advancement. J Manuf Syst 2022; 63:504–5.
[20] Fang F. Atomic and close-to-atomic scale manufacturing: perspectives and measures. Int J Extreme Manuf 2020;2:030201.
[21] Xie W, Fang F. Rake angle effect in cutting-based single atomic layer removal. J Manuf Process 2020;56:280–94.
[22] Krivanek OL, Tsui D, Sheng T, Kamgar A. A high resolution electron microscopy study of the $Si-SiO_2$ interface. In: The physics of SiO_2 and its interfaces. Elsevier; 1978. p. 356–61.
[23] Akatsu H, Ohdomari I. HRTEM observation of the Si/SiO_2 interface. Appl Surf Sci 1990;41:357–64.
[24] Yoshinobu T, Iwamoto A, Sudoh K, Iwasaki H. Scaling of Si/SiO_2 interface roughness. J Vac Sci Technol B Microelectron Nanometer Struct Process Meas Phenom 1995;13:1630–4.
[25] Bongiorno A, Pasquarello A. Validity of the bond-energy picture for the energetics at $Si-SiO_2$ interfaces. Phys Rev B 2000;62:R16326.
[26] Tu Y, Tersoff J. Structure and energetics of the $Si-SiO_2$ interface. Phys Rev Lett 2000;84:4393.
[27] Deal BE. The current understanding of charges in the thermally oxidized silicon structure. J Electrochem Soc 1974;121:198C.
[28] Kageshima H, Shiraishi K, Uematsu M. Universal theory of Si oxidation rate and importance of interfacial Si emission. Jpn J Appl Phys 1999;38:L971.
[29] Uematsu M, Kageshima H, Shiraishi K. Unified simulation of silicon oxidation based on the interfacial silicon emission model. Jpn J Appl Phys 2000;39:L699.
[30] Kageshima H, Shiraishi K. First-principles study of oxide growth on Si (100) surfaces and at SiO_2/Si (100) interfaces. Phys Rev Lett 1998;81:5936.
[31] Bottomley D, Omi H, Kobayashi Y, Uematsu M, Kageshima H, Ogino T. Origin of self-assembled step and terrace formation at the Si (001)– SiO 2 interface. Phys Rev B 2002;66:035301.
[32] Acosta-Alba PE, Kononchuk O, Gourdel C, Claverie A. Surface self-diffusion of silicon during high temperature annealing. J Appl Phys 2014;115:134903.
[33] Omi H, Kageshima H, Kawamura T, Uematsu M, Kobayashi Y, Fujikawa S, et al. Stability-instability transition of reaction fronts in thermal oxidation of silicon. Phys Rev B 2009;79:245319.
[34] Li Y-F, Liu Z-P. Smallest stable Si/SiO_2 interface that suppresses quantum tunneling from machine-learning-based global search. Phys Rev Lett 2022;128:226102.
[35] Omi H, Kageshima H, Uematsu M. Scaling and universality of roughening in thermal oxidation of Si (001). Phys Rev Lett 2006;97:016102.
[36] Omi H, Homma Y. Self-ordering on vicinal Si (111) during molecular beam epitaxy. Phys Rev B 2005;72:195322.
[37] Kageshima H, Shiraishi K, Endoh T. Reconsideration of Si pillar thermal oxidation mechanism. Jpn J Appl Phys 2018;57:06KD02.
[38] Hojo D, Tokuda N, Yamabe K. Direct observation of two-dimensional growth at SiO_2/Si (111) interface. Thin Solid Films 2007;515:7892–8.
[39] Solà Garcia MM. Fabrication of c-Si microstructures through reorganization at high temperatures, in. Universitat Politècnica de Catalunya; 2015.
[40] Salvalaglio M, Backofen R, Voigt A, Montalenti F. Morphological evolution of pit-patterned Si (001) substrates driven by surface-energy reduction. Nanoscale Res Lett 2017;12:1–8.
[41] Liang S, Zhang L, Deng H. Theoretical and experimental study on plasma-induced atom-migration manufacturing (PAMM) of glass. Appl Surf Sci 2022;599:153976.
[42] Li R, Li Y, Deng H. Plasma-induced atom migration manufacturing of fused silica. Precis Eng 2022;76:305–13.
[43] Zhou Y, Zhou J, Tian Z, Dong F, Liu S, Wang J. Improving the crystal quality of AlN films by nanosecond laser annealing. J Manuf Process 2022;84:1519–25.
[44] Sarani A, Nikiforov AY, Leys C. Atmospheric pressure plasma jet in Ar and Ar/H_2O mixtures: optical emission spectroscopy and temperature measurements. Phys Plasmas 2010;17:063504.
[45] Song M, Lee Y, Chung T. Characterization of an inductively coupled nitrogen-argon plasma by Langmuir probe combined with optical emission spectroscopy. Phys Plasmas 2011;18:023504.
[46] Battersby CL, Sheehan LM, Kozlowski MR. Effects of wet etch processing on laser-induced damage of fused silica surfaces. In: Laser-induced damage in optical materials: 1998. SPIE; 1999. p. 446–55.
[47] Bouchut P, Garrec P, Pelle C. Wet etching for the mitigation of laser damage growth in fused silica. In: Laser-induced damage in optical materials: 2002 and 7th international workshop on laser beam and optics characterization. SPIE; 2003. p. 103–11.
[48] Wong L, Suratwala T, Feit M, Miller P, Steele R. The effect of HF/NH4F etching on the morphology of surface fractures on fused silica. J Non-Cryst Solids 2009;355: 797–810.
[49] Proksche H, Nagorsen G, Ross D. The influence of NH4F on the etch rates of undoped SiO_2 in buffered oxide etch. J Electrochem Soc 1992;139:521.